# Nucleate Pool Boiling Heat Transfer Measurement and Flow Visualization for Ammonia-Water Mixture

**A. Sathyabhama**[1]
Research Scholar
Department of Mechanical Engineering NITK, Surathkal/Faculty MSRIT, Vidya Soudha, MSR Nagar, MSRIT Post, Bangalore-560 054, Karnataka, India
e-mail: sathyabhamaa@hotmail.com

**T. P. Ashok Babu**
Professor
Department of Mechanical Engineering NITK, Surathkal Post Srinivasnagar, Mangalore 575 025, Karnataka, India

*Visualization of bubble nucleation during nucleate pool boiling outside a vertical cylindrical heated surface was done for ammonia-water binary mixture in order to obtain a descriptive behavior of the boiling, which was directly compared with the measured heat transfer coefficient data at low pressure of 4–8 bar and at low mass fraction of $0 < x < 0.3$ and at different heat flux. Still images taken with high speed camera are used to demonstrate the decrease in boiling heat transfer coefficient with increase in ammonia mass fraction. Jensen and Memmel model has better agreement with experimental bubble diameter. Further work is required to obtain quantitative information about bubble nucleation parameters. It is found that both Calus and Rice and Stephan–Koorner correlation can predict the experimental heat transfer coefficient values with a maximum deviation of $\pm$ 20%.* [DOI: 10.1115/1.4004258]

*Keywords: ammonia/water, pool boiling, heat transfer coefficient, bubble dynamics, visualization*

## Introduction

Ammonia/water absorption refrigerating systems are receiving an increasing attention as an environmentally safe replacement for the CFC-based compression cycles. This has created increasing research activities in pool boiling heat transfer of this mixture. However, detailed literature review shows that experimental data on boiling heat transfer coefficients of ammonia/water mixture are scarce. Mixture boiling heat transfer correlations with acceptable level of accuracy have been reported and validated extensively. However, in the case of ammonia-water mixture there is still an important lack of fundamental and empirical information.

Boiling of mixtures is distinct from boiling of pure liquids in that the driving force for heat transfer is in turn governed by mass transfer. Therefore, the evaporation rate can be severely reduced for the mixtures because the rate of mass diffusion in the liquid phase is usually much slower than that of heat diffusion. Van Wijk et al. [1] presented the physical explanation for the observed reduction of the mixture boiling heat transfer coefficient. They suggested that preferential evaporation of the more volatile component takes places at the heated surface such that the local boiling point rises. Sternling and Tichacek [2] provided three possible explanations:

(1) the change in the mixture physical properties, notably viscosity with composition.
(2) the change in the rate of bubble growth caused by the resistance to the mass transfer of the more volatile component in diffusing into the growing bubble, and
(3) changes in the rate of nucleation of new boiling sites on the surface.

According to the work of Thome [3,4], the decrease in the boiling heat transfer coefficient is a combined result of mixture effects on bubble growth rate, bubble departure diameter and boiling site density, and nonlinear variation of the pertinent physical properties.

The primary objective of this work is to obtain experimental data for saturated pool boiling of ammonia-water mixture at varying mass fraction of ammonia. The experimental data obtained also include the influence of pressure and heat flux on heat transfer rate. The present investigation also aims at obtaining a visual record of nucleation to demonstrate the degradation of boiling heat transfer with increase in ammonia mass fraction.

## Experimental Setup

The schematic diagram of experimental setup is shown in Fig. 1. The unit consists of boiling vessel, water pump, vacuum pump, condenser coil, and test section. Boiling vessel 80 mm diameter and 200 mm long made up of SS 316 is fitted with SS 316 flanges at the top and at the bottom as shown in Fig. 1. The vessel is fitted with two sight glasses to observe and record the boiling phenomena. The top flange has provisions for liquid charging, condenser cooling water inlet and outlet, vacuum pump, pressure transducer, and thermocouples to measure liquid and vapor temperatures. Bottom flange has provisions for test section and drain. The test section is a rod heater mounted vertically within the boiling vessel. Boiling takes place at the outer surface of a cylindrical alloy steel rod with a diameter of 6 mm and a heating length of 20 mm. The test section is heated by an electrical heating element of 1 kW capacity. The heating element is connected to a wattmeter through a dimmer stat to read the power supplied to it. The details of the test heater are given in Fig. 2.

A high speed camera (Nikon D3) was used to take the photographs of the pool boiling on the outer surface of vertical heater inside the boiling vessel. The camera was positioned infront of the sight glass. A concentrated light source was placed infront of another sight glass opposite to the camera to give uniform illumination of the test heater.

All temperatures of the system are measured using chrome alumel K type thermocouples. Two thermocouples are set in the liquid pool and vapor, respectively. These liquid and vapor temperatures confirm the system being maintained at the saturation state during

[1]Corresponding author.

Contributed by the Heat Transfer Division of ASME for publication in the Journal of Heat Transfer. Manuscript received May 28, 2010; final manuscript received May 16, 2011; published online August 23, 2011. Assoc. Editor: Srinivas Garimella.

  

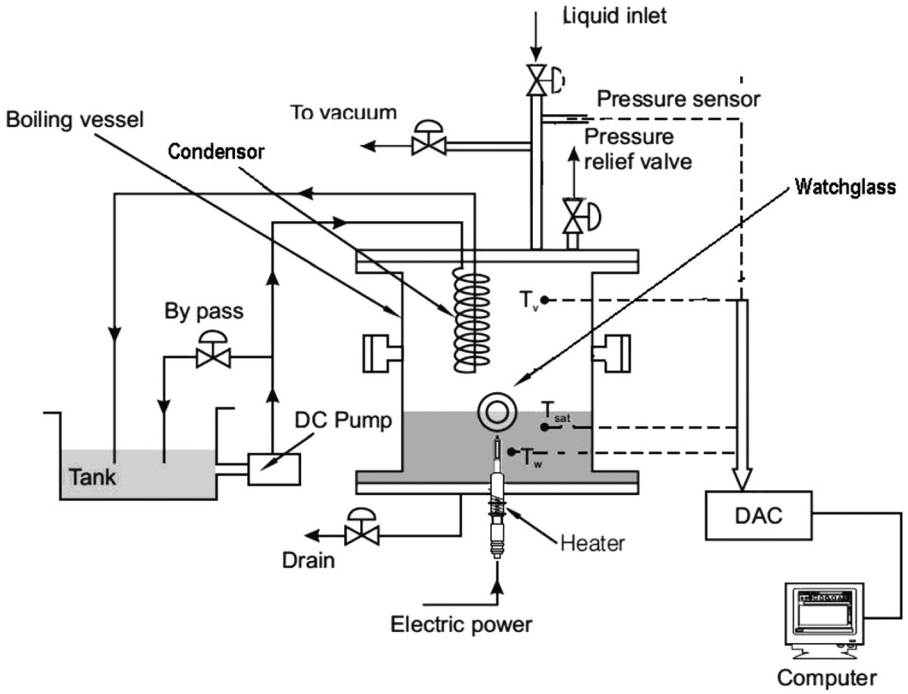


**Fig. 1 Schematic diagram of experimental setup**

the experiments. Two thermocouples are embedded along the circumference of the heater close to the heating surface. The surface temperature is calculated by correcting the minor temperature drop due to the small distance between the heating surface and the thermocouple location using Fourier heat conduction equation. The internal pressure of boiling vessel is measured by a pressure transducer. The power input to the test heater is measured using a wattmeter. The boiling vessel is well insulated. Electrical signals from the thermocouples, pressure transducer, and wattmeter are processed by a data acquisition system.

## Experimental Procedure

In order to start the boiling tests, the boiling vessel should be filled with the ammonia-water mixture. Before filling the chamber with the mixture, it was evacuated using a vacuum pump. The pressure of the boiling vessel was read on the logger display. Once the evacuation process was completed, the boiling vessel was filled with ammonia-water mixture. Commercially available ammonia-water mixture is used in this work. Concentration is measured by titration and the repeatability in the concentration measurement is $\pm$ 0.3%. The amount of mixture was chosen so as to maintain a fixed level in all experiments. The test pressure was set in the logger and the mixture was heated to corresponding saturation temperature. When the system reached steady state, the tests were started by varying heat input to the test heater. The magnitude of the heat input was known from the wattmeter. All experimental runs were carried out with decreasing heat flux to avoid the hysteresis effect. Some runs were repeated twice and even thrice to ensure the reproducibility of the experiments. To demonstrate the reproducibility of the experimental data, several tests for pure components and mixtures were repeated on the same surface throughout the testing life of the heaters. These tests confirmed that the heat transfer coefficient values were repeatable within 7.2%. A high speed camera was used to film the boiling process simultaneously with the heat transfer measurements.

**Calculations.** Heat input $Q$ is a known quantity as there can be no losses because the test heater is completely immersed in the liquid. Then heat flux, $q = Q/A$, where $A$ is the surface area of the test section. $A = \pi dL$, where d is the diameter of the heater rod and $L$ is the heating length of the heater rod. Heat transfer coefficient between the surface and the liquid is calculated by applying Newton's law of cooling

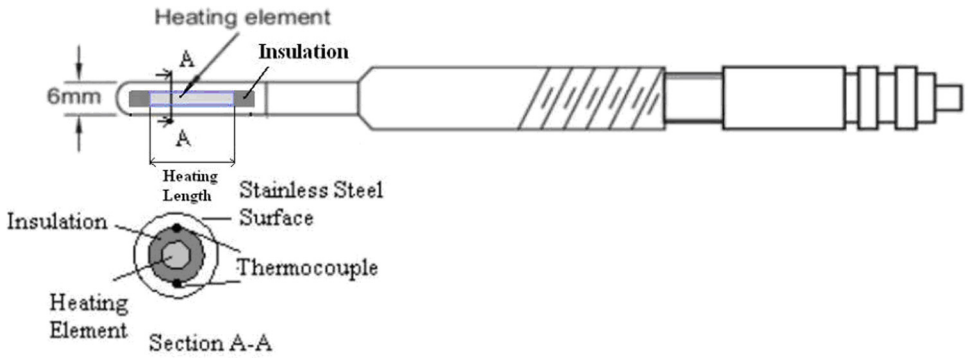


**Fig. 2 Details of test heater**

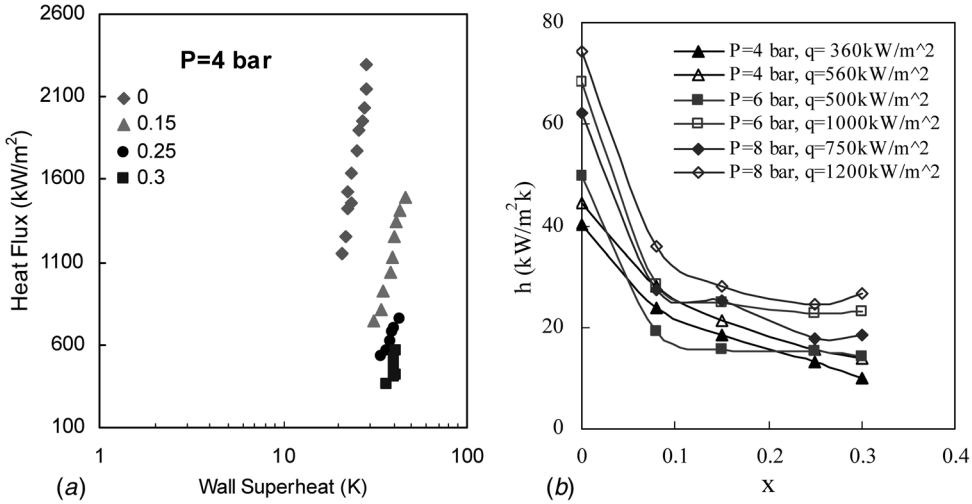


**Fig. 3 (*a*) Boiling curve at 4 bar pressure and (*b*) effect of ammonia mass fraction on heat transfer coefficient**

$$h = \frac{q}{T_w - T_s} \tag{1}$$

where $T_s$ is the saturation temperature of the liquid at the corresponding pressure and $T_w$ is the surface temperature of the test.

## Experimental Uncertainty

All chrome alumel K type thermocouples used in this study have an accuracy of ±0.5% full scale. The internal pressure of boiling vessel is measured by a pressure transducer with an uncertainty of ±0.01 bar. The power input to the heater is measured by an accurate digital power meter with ±1 W uncertainty. The uncertainty in temperature measurement was ±1.25 °C. Uncertainty in length and diameter measurement was ±0.1 mm. The resulting uncertainty in the area of the heated surface was 1.74%. The Kline and McClintock [5] technique was used to estimate the uncertainty for the derived quantities. The resulting maximum uncertainty in the heat flux was 1.94%. The maximum uncertainty in the wall superheat values was 10.71%. The maximum uncertainty in the heat transfer coefficient was 10.86%.

## Experimental Results

Validation of the experimental setup for the pure water boiling is discussed in Ref. [6]. Figure 3(*a*) shows the boiling curve at 4 bar pressure. Boiling curve shifts to the right with increase in ammonia mass fraction. Figure 3(*b*) shows the effect of ammonia mass fraction on heat transfer coefficient. For a constant heat flux, heat transfer coefficient reduces with increase in ammonia mass fraction in the investigated range. For a given pressure heat transfer coefficient increases with increase in heat flux. For constant mass fraction, heat transfer coefficient increases with increase in both pressure and heat flux.

## Comparison of Correlations With the Measured Data

The measured heat transfer coefficient data were compared with correlations of Stephan–Koorner [7], Thome and Shakir [8], Fujita–Tsutsui [9], and Calus and Rice [10]. These correlations are listed in Table 1.

The ideal heat transfer coefficient in the above equations is given by

$$h_{id} = \frac{1}{\frac{x_1}{h_1} + \frac{x_2}{h_2}} \tag{6}$$

Correlation of Mostinski [11] given by Eq. (7) is used to calculate the ideal heat transfer coefficient in this work.

$$h = 0.00417 q^{0.7} P_c^{0.69} F_{\mathrm{PF}} \tag{7}$$

where $F_{\mathrm{PF}}$ is a nondimensional pressure correction factor that characterizes pressure effects on nucleate boiling as

$$F_{\mathrm{PF}} = 1.8 p_r^{0.17} + 4 p_r^{1.2} + 8 p_r^{10} \tag{8}$$

The correlation of Stephan–Koorner is shown plotted in Fig. 4. Stephan–Koorner correlation for mixtures contains the composition difference between the vapor and liquid phases, ($y_i - x_i$) to account for the mixture effect. Stephan and Korner determined the value of $A_o$, the empirical constant to range from 0.42 to 3.56, for 17 mixtures by fitting Eq. (2) to the measured data. Their average value of 1.53 is recommended for mixtures whose data are not available. Agreement between the measured heat transfer coefficient and Stephan–Koorner correlation is ±20%. Thome and Shakir combine the boiling range and the mass diffusion effects to account for mixture effects. $B_o$, the scaling factor, is equated to unity on the assumption that all the heat transfer from the heated

**Table 1 Nucleate boiling correlations for mixture**

| | | |
|---|---|---|
| Stephan and Koorner [7] | $\frac{h}{h_{id}} = [1 + A_o(0.88 + 0.12P)(y_1 - x_1)]^{-1}$ | (2) |
| Thome and Shakir [8] | $\frac{h}{h_{id}} = \left\{1 + \frac{h_{id}}{q}\Delta T_{bp}\left[\left(1 - \exp\frac{-B_o q}{\rho_L h_{fg} \beta_L}\right)\right]\right\}^{-1}$ | (3) |
| Fujita–Tsutsui [9] | $\frac{h}{h_{id}} = \left\{1 + \frac{\Delta T_{bp}}{\Delta T_{id}}\left[1 - \exp\left(\frac{-60q}{\rho_v h_{fg}}\left\{\frac{\rho_v^2}{\sigma g(\rho_L - \rho_v)}\right\}^{1/4}\right)\right]\right\}^{-1}$ | (4) |
| Calus and Rice [10] | $\frac{h}{h_{id}} = \left[\left\{1 + (y_1 - x_1)\left(\frac{\alpha_L}{D}\right)^{0.5}\right\}^{0.7}\right]^{-1}$ | (5) |

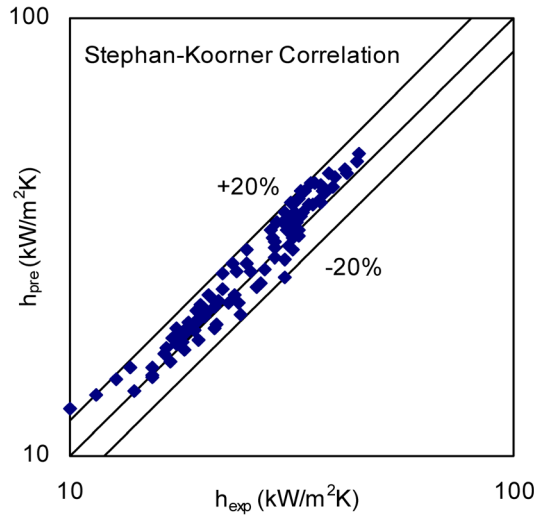


**Fig. 4 Comparison of Stephan–Koorner correlation with experimental data**

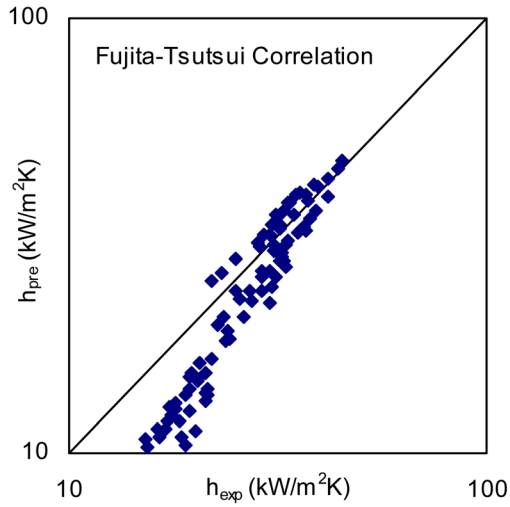


**Fig. 6 Comparison of Fujita–Tsutsui correlation with experimental data**

surface in nucleate boiling passes into the bubble in the form of latent heat. They assigned a fixed value of 0.0003 m/s for $\beta_L$, the liquid side mass transfer coefficient. The correlation of Thome and Shakir underpredicts the experimental values and the deviation is not systematic as can be seen from Fig. 5. A plot is drawn in Fig. 6 between the experimental data and the predictions from Fujita–Tsutsui correlation that is based on a model that the drop of effective temperature difference is a main reason for heat transfer reduction in mixtures. Good agreement is achieved between the measured heat transfer coefficient and Fujita–Tsutsui correlation at very low mass fraction of ammonia but the deviation increases with increase in ammonia mass fraction. One of the few correlations to attempt to quantitatively relate the reduction in heat transfer coefficient to the reduction in bubble growth rate is that of Calus and Rice. Their correlation involves the diffusion coefficient D and as can be seen from Fig. 7 the correlation can predict the present experimental data within ±20%.

**Nucleation.** Even though nucleation behavior has been studied for pool boiling, there is no generally accepted model to explain bubble growth behavior due to the complexity of boiling heat transfer. Zhao and Tsuruta [12] studied bubble growth behavior and developed the micro layer theory. The cycle of a bubble consists of two parts, one being the lifetime and other is the waiting time of nucleus activity. As reported by Zhao and Tsuruta, the lifetime of the individual bubble consist of three durations: initial growth duration, final growth duration, and the condensation duration before the individual bubble collapses. To understand the phases of the bubble growth at the nucleation sites, a high speed camera was used. Because the bubbles rise and collapse very quickly, it is a tough task to identify the exact growth process of bubbles rising from the heater surface.

The experiments conducted in this study are at high heat flux and at relatively high pressure. At these pressures and heat flux isolation of single bubble on the surface could not be done for study due to vigorous interaction with other bubbles. Consequently, the comparison of bubble nucleation at different pressure, heat flux, and ammonia mass fraction is mostly visual and subjective. Bubble nucleation parameters were not clearly measurable, due to the much greater density of nucleation sites on the heater surface considered in this work. The exact timing of bubble departure events could not be marked, as the growing bubbles moved from their nucleation sites while still being attached to the surface,

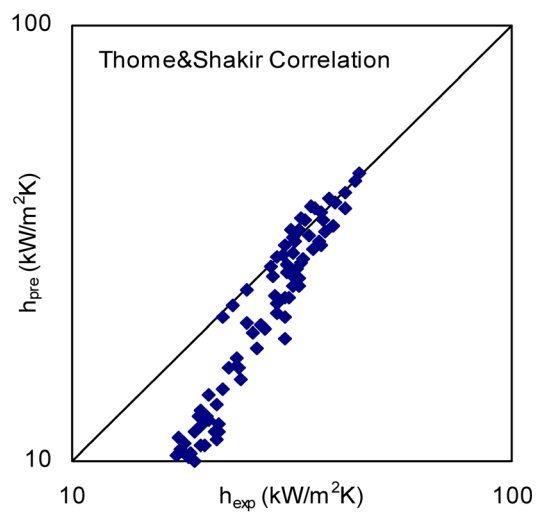


**Fig. 5 Comparison of Thome and Shakir correlation with experimental data**

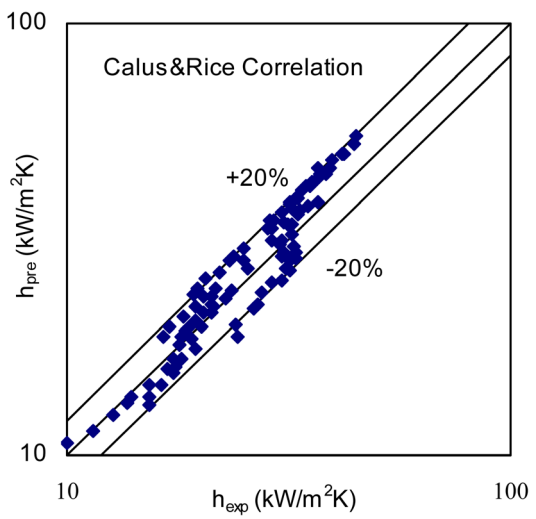


**Fig. 7 Comparison of Calus and Rice correlation with experimental data**

**Table 2 Bubble size**

| | $x = 0.25$ | | | $x = 0.30$ | | |
|---|---|---|---|---|---|---|
| | $P = 4$ bar | $P = 6$ bar | $P = 8$ bar | $P = 4$ bar | $P = 6$ bar | $P = 8$ bar |
| $q = 500$ kW/m$^2$ | 0.90 mm | 0.80 mm | 0.70 mm | 0.87 mm | 0.77 mm | 0.68 mm |
| $q = 750$ kW/m$^2$ | 1.40 mm | 0.90 mm | 0.80 mm | 1.25 mm | 0.86 mm | 0.78 mm |

either by merger with a larger neighboring bubble or by sliding along the vertical surface in to the bulk flow. Only representative average bubble diameter was measured. The bubble diameter was obtained by measuring both the bubble diameter and the sight glass from the image using a MATLAB program and scaling down to obtain bubble diameter from the known sight glass diameter. The uncertainty in bubble diameter measurement is $\pm 1$ pixel (each pixel is approximately 12.65 $\mu$m, determined using the known sight glass diameter after taking a suitable correction factor for the relative distance of 90 mm between the test surface and the sight glass). The bubble diameter reported is the average of the values obtained for 20 bubbles in each image. The contact angle, the site density and the bubble frequency could not be measured due to the above said reason.

Figures 8(*a*)–8(*f*) shows the flow situation on the heated surface at different pressures, change of flow aspect with heat flux and change with the mass fraction. Sample bubble images at different conditions are presented for comparison. The average bubble size measured at different pressures, heat flux and ammonia mass fraction are given in Table 2.

**Effect of Heat Flux.** It is observed that bubble diameter at detachment increases with an increase in heat flux. The same flow pattern is observed for another pressure and another mass fraction. Increase of nucleation site and frequency of bubble formation are clearly observed. It is found that as the heat flux increases the bubbles begin coalescing, which are generated on the adjoining nucleation site on the heated surface. It is observed that at higher heat flux, the nucleation rate is so high that the bubbles seem to leave the surface in clusters, but, in fact, they are individual bubbles leaving heater surface. Also, observation from Fig. 8 reveals that the bubbles are mostly spherical in shape and seem to be nucleating uniformly.

**Effect of Pressure.** In the case of increase in pressure, the detached bubble diameter decreases, frequency of bubble formation increases. The net effect is increase in boiling heat transfer coefficient.

**Effect of Mass Fraction.** Figure 8 also clearly implies that bubble behavior is dependent on the mass fraction in nucleate boiling of mixtures. The composition for binary mixture has an important effect on the boiling site density, bubble departure diameter, and bubble departure time. In this study, this is obvious that the increase in mass fraction of ammonia causes the bubble departure diameter and the bubble departure frequency to be

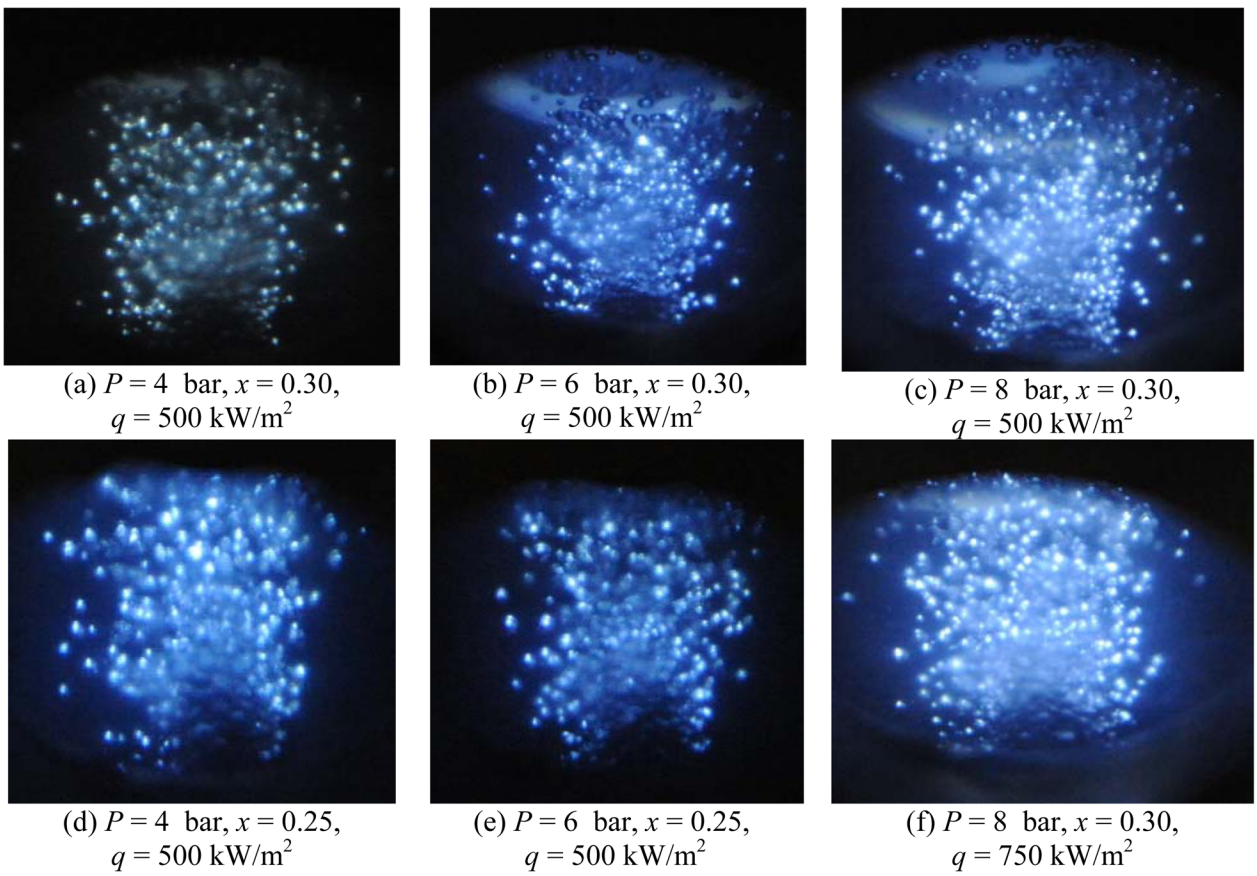


**Fig. 8 Visual record of boiling phenomena**

**Table 3 Correlations of bubble departure diameter**

| | | |
|---|---|---|
| Fritz [13] | $D_d = 0.0208\theta\left[\frac{\sigma}{g(\rho_L - \rho_v)}\right]^{1/2}$ | (9) |
| Cole and Shulman [14] | $D_d = \sqrt{\frac{\sigma}{g(\rho_L - \rho_v)}}\frac{1000}{P}$ $P$ in mm of Hg | (10) |
| Cole [15] | $D_d = 0.04\mathrm{Ja}\left[\frac{2\sigma}{g(\rho_L - \rho_v)}\right]^{1/2}$ | (11) |
| Van Stralen et al. [16] | $D_d = 2.63\left(\frac{\mathrm{Ja}^2\alpha_L^2}{g}\right)^{1/3}\left[1 + \left(\frac{2\pi}{3\mathrm{Ja}}\right)^{1/2}\right]^{1/4}$ | (12) |
| Kutateladze and Gogonin [17] | $D_d = 0.25\left(1 + 10^5 K_L\right)^{1/2}\left[\frac{\sigma}{g(\rho_L - \rho_v)}\right]^{1/2}$ for $\mathrm{Kl} < 0.06$ | (13) |
| | $K_L = \left(\frac{\mathrm{Ja}}{\mathrm{Pr}_L}\right)\left(\left\{\left[\frac{g\rho_L(\rho_L - \rho_v)}{\mu_L^2}\right]\right\}\left[\sqrt{\frac{\sigma}{g(\rho_L - \rho_v)}}\right]^{3/2}\right)^{-1}$ | (14) |
| Jensen and Memmel [18] | $D_d = 0.19\left(1.8 + 10^5 K_L\right)^{2/3}\left[\frac{\sigma}{g(\rho_L - \rho_v)}\right]^{1/2}$ <br> $K_L = \left(\frac{\mathrm{Ja}}{\mathrm{Pr}_L}\right)\left(\left\{\left[\frac{g\rho_L(\rho_L - \rho_v)}{\mu_L^2}\right]\right\}\left[\sqrt{\frac{\sigma}{g(\rho_L - \rho_v)}}\right]^{3/2}\right)^{-1}$ | (15) |

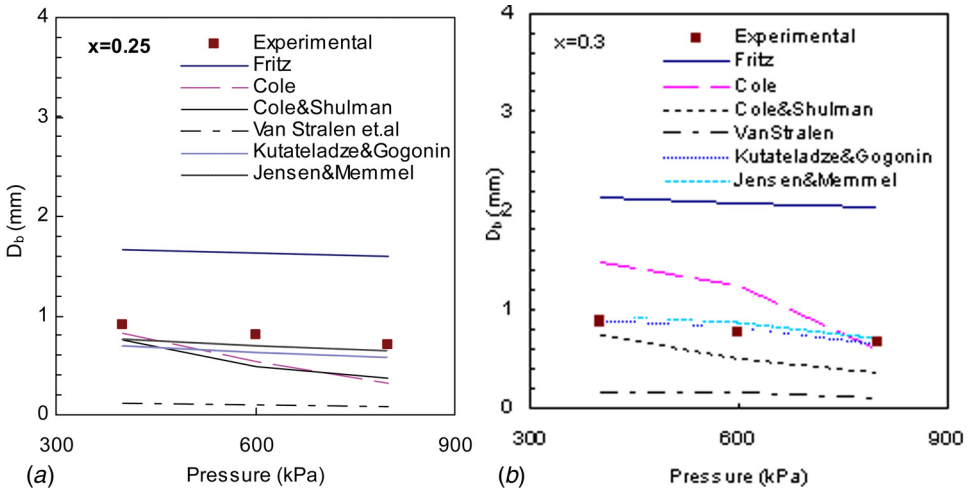


**Fig. 9 (*a*) and (*b*) Comparison between the measured bubble diameter and predicted bubble diameter from the correlations**

decreased in most cases and these two parameters result in the degradation of the heat transfer coefficient in the regions of high ammonia mass fractions.

Many correlations are developed for the prediction of the bubble diameter for the nucleate pool boiling condition for different applications. The Fritz [13] model, which assumes that there is a balance between surface tension and buoyancy forces at the moment of departure is one of the most reliable existing models for prediction of the bubble diameter for boiling of pure liquids and also liquid mixtures. Cole and Shulman [14] proposed a relation in which bubble diameter is simply proportional to the inverse of the absolute pressure. Cole [15] modified the contact angle and proposed that the effect of system pressure is involved through a modified Jacob number. Van Stralen and Zijl [16] proposed an empirical model for nucleate boiling based on bubble growth mechanisms. This model includes the Jakob number and thermal diffusivity of the solution. Kutateladze and Gogonin [17] could correlate a large body of data from the literature with the correlation given in Eq. (13). Jensen and Memmel [18] proposed an improvement to Eq. (13) with their correlation (Eq. (15)). The bubble departure diameter correlations selected in this work are listed in Table 3. All of the above correlations for departure bubble size at various pressures are plotted in Fig. 9(*a*) for ammonia mass fraction of 0.25 and in Fig. 9(*b*) for ammonia mass fraction of 0.3. The results clearly show an inverse trend with pressure. Because accurate values of the contact angle are very difficult to measure experimentally, an average value of 35 deg is assumed in Fritz correlation. As can be seen in the figures, Fritz correlation overpredicts the experimental data. This is because Fritz correlation is valid only in the region of atmospheric pressure and at low heat flux levels. Van Stralen model underpredicts the experimental data. Correlation of Cole and those similar to it are promising in that the Jakob number accounts for pressure and superheat variations. Kutateladze and Gogonin and Jensen and Memmel models suggest that the bubble departure diameter is a weaker function of Jakob number. This has led to a better agreement of their models with the present experimental results, especially in the case of the Jensen and Memmel model for which the variation trend with pressure closely follows the experimental results.

## Conclusion

Nucleate pool boiling heat transfer coefficient of ammonia-water binary mixture was measured at low pressures of 4 bar to 8 bar and at low ammonia mass fraction of $0 < x < 0.3$ and at different heat flux. Degradation of heat transfer was observed with increase in ammonia mass fraction in the investigated range. Experiments should be extended to whole range of mass fraction of ammonia. Measured heat transfer coefficient fairly agrees with the predictions from Stephan–Koorner and Calus and Rice correlations with a deviation of $\pm 20\%$. A visual recording of the nucleation was obtained at saturated boiling conditions with varying heat flux, pressure and at two different ammonia mass fractions. Observations from visual recordings reveal that bubble size decreases with increase in pressure and ammonia mass fraction in the investigated range. Jensen and Memmel model predicts the bubble diameter with reasonable accuracy. Further investigation is required to measure the bubble parameters quantitatively.

## Nomenclature

$A$ = area ($m^2$)
$A_o$ = constant in Eq. (2)
$B_o$ = scaling factor in Eq. (3)
CFC = Chlorofluorocarbon
$cp$ = specific heat (J/kgK)
$D$ = mass diffusivity ($m^2s^{-1}$)
$D_d$ = bubble departure diameter (m)
$g$ = gravitational acceleration ($ms^{-2}$)
$h_{fg}$ = latent heat of vaporization (J $kg^{-1}$)
$h$ = nucleate boiling heat transfer coefficient (W $m^{-2}$ $K^{-1}$)
Ja = Jakob number $\frac{\rho_L cp_L (T_w - T_s)}{\rho_v h_{fg}}$
$P$ = pressure (bar)
$P_c$ = critical pressure (bar)
Pr = Prandtl number $\frac{\mu cp}{k}$
$p_r$ = reduced pressure
$Q$ = heat input
$q$ = heat flux (W $m^{-2}$ $K^{-1}$)
SS = Stainless steel
$T$ = temperature (K)
$x$, $y$ = mass fraction of liquid and vapor

## Greek Symbols

$\alpha$ = thermal diffusivity ($m^2s^{-1}$)
$\beta$ = mass transfer coefficient ($ms^{-1}$)
$\Delta T$ = temperature difference (K)
$\mu$ = dynamic viscosity (Pa.s)
$\rho$ = density ($kgm^{-3}$)
$\sigma$ = surface tension ($Nm^{-1}$)
$\theta$ = contact angle (deg)

## Subscripts

i = volatile component
id = ideal
L = liquid
s = saturation
v = vapor
w = wall

## References


[1] Van Wijk, W. R., Vos, A. S., and Van Stralen, J. D., 1956, "Heat Transfer to Boiling Binary Liquid Mixtures," Chem. Eng. Sci., **5**, pp. 68–80.
[2] Sternling, C. V., and Tichacek, L. J., 1961, "Heat Transfer Coefficients for Boiling Mixtures," Chem. Eng. Sci., **16**, pp. 297–337.
[3] Thome, R., 1978, "Bubble Growth and Nucleate Pool Boiling in Liquid Nitrogen, Argon and Their Mixtures," Ph.D. thesis, Oxford University, UK.
[4] Thome, J. R., 1982, "Latent and Sensible Heat Transfer Rates in Boiling of Binary Mixtures," ASME J. Heat Transfer, **104**, pp. 474–478.
[5] Kline, S. J., and McClintock, F. A., 1953, "Describing Uncertainties in Single-Sample Experiments," Mech. Eng., **75**, pp. 3–8.
[6] Sathyabhama, A., and Ashok Babu, T. P., 2011, "Experimental Investigation in Pool Boiling Heat Transfer of Ammonia/Water Mixture and Heat Transfer Correlations," Int. J. Heat Fluid Flow, **32**, pp. 719–729.
[7] Stephan, K., and Korner, M., 1969, "Calculation of Heat Transfer in Evaporating Binary Liquid Mixtures," Chem.-Ing.-Tech., **41**(7), pp. 409–417.
[8] Thome, J. R., and Shakir, S., 1987, "A New Correlation for Nucleate Pool Boiling of Aqueous Mixtures," AIChE Symp. Ser., **83**(257), pp. 46–51.
[9] Fujita, Y., and Tsutsui, M., 1997, "Heat Transfer in Nucleate Boiling of Binary Mixtures (Development of a Heat Transfer Correlation)," JSME Int. J., Ser. B, **40**, pp. 134–141.
[10] Calus, W. F., and Rice, P., 1972, "Pool Boiling–Binary Mixtures," Chem. Eng. Sci., **27**, pp. 1687–1697.
[11] Mostinski, I. L., 1963, "Application of the Rule of Corresponding States for Calculation of Heat Transfer and Critical Heat Flux," Teploenergetika, **10**(4), pp. 66–71.
[12] Zhao, Y., and Tsuruta, T., 2002, "Prediction of Bubble Behavior in Subcooled Pool Boiling Based on Microlayer Model," JSME Int. J., Ser. B, **45**(2), pp. 346–354.
[13] Fritz, W., 1935, "Berechnung des maximalvolume von dampfblasen," Phys. Z., **36**, pp. 379–388.
[14] Cole, R., and Shulman, H. L., 1966, "Bubble Departure Diameters at Subatmospheric Pressures," Chem. Eng. Prog., **62**, pp. 6–16.
[15] Cole, R., 1967, "Bubble Frequencies and Departure Volumes at Subatmospheric Pressures," AIChE J., **13**, pp. 779–783.
[16] Van Stralen, S. J. D., and Zijl, W., 1978, "Fundamental Developments in Bubble Dynamics," *Proceedings of the Sixth International Heat Transfer Conference*, Toronto, Vol. 6, pp. 429–450.
[17] Kutateladze, S., and Gogonin, I., 1980, "Growth Rate and Detachment Diameter of a Vapor Bubble in Free Convection Boiling of a Saturated Liquid," High Temp., **17**, pp. 667–671.
[18] Jensen, M. K., and Memmel, G. J., 1986, "Evaluation of Bubble Departure Diameter Correlations," *Proceedings of the Eighth International Heat Transfer Conference*, Vol. 4. pp. 1907–1912.